J. Fluid Mech. (1991), *vol.* 222, *pp.* 267–291
Printed in Great Britain

Nonlinear perturbation of the vortex shedding from a circular cylinder

By GIANCARLO ALFONSI[1] AND ALDO GIORGINI[2]

[1] Istituto di Idraulica, Politecnico di Milano, Piazza Leonardo da Vinci 32, 20133 Milano, Italy
[2] School of Civil Engineering, Purdue University, West Lafayette, IN 47907, USA

(Received 28 November 1988 and in revised form 15 January 1990)

The influence of finite-amplitude perturbations on the unsteady vortex shedding past an impulsively started circular cylinder is investigated by means of a numerical model. The computational scheme is a mixed spectral–finite analytic technique, in which the fast-Fourier-transform algorithm is used for the evaluation of the nonlinear terms in the two-dimensional time-dependent Navier–Stokes equations in their stream function–vorticity transport form (the Helmholtz formulation) at $Re = 1000$. The vortex shedding is promoted by imposing at $t = 0$ a small rotational field to the initially irrotational flow. Attention is focused on the strength of the perturbation vortex, which affects the way in which the vortex shedding develops in time. The results of the simulations are presented by means of computer-generated drawings of absolute streamlines, relative streamlines and vorticity fields; it appears that, when the strength of the initial perturbation assumes the minimum value that has been tested, the vortex shedding phenomenon develops in a way different from that resulting from other numerical experiments of the same kind.

1. Introduction

There has been a considerable number of theoretical studies on vortex shedding past a circular cylinder, and amongst them the works of Bairstow, Cave & Lang (1922, 1923), Thom (1932), Roshko (1953, 1954), Abernathy & Kronauer (1962), Smith (1979, 1981), Cowley (1983), Tamada, Miura & Miyagi (1983) and Triantafyllou, Triantafyllou & Chryssostomidis (1986), should be mentioned as relevant to the present study.

At the same time, numerical solutions started to appear, mainly based on finite-difference implicit schemes but also on finite-element and boundary-element methods, and related to both steady and unsteady flows and symmetric and non-symmetric configurations of the wake. A list of such works is reported in table 1, together with the maximum value of the Reynolds number reached in the calculations.

An analysis of the existing literature shows that there has been relatively little numerical research on the flow around a circular cylinder at Reynolds numbers higher than 500, the non-steady case has been investigated only for small time steps, the majority of the work has been done on symmetric flow, and poor analysis of the near-wake characteristics is provided. More recently, spectral numerical methods have started to appear, mainly due to both their accuracy and the increasing availability of supercomputers. Spectral analysis based on a Fourier series expansion

Author(s)	*Re* (max.)	Author(s)	*Re* (max.)
Steady flow		Unsteady flow	
Thom (1933)	20	Payne (1958)	100
Kawaguti (1953)	40	Kawaguti & Jain (1966)	100
Allen & Southwell (1955)	1000	Ingham (1968)	100
Apelt (1958)	44	Jain & Sankara Rao (1969)	200
Keller & Takami (1966)	15	Son & Hanratty (1969)	500
Hamielec & Raal (1969)	500	Thoman & Szewczyk (1969)	300000
Takami & Keller (1969)	60	Jordan & Fromm (1972)	1000
Tuann & Olson (1978)	100	Wu & Thompson (1973)	120
Fornberg (1980)	300	Okajima, Takata & Asanuma (1975)	6100
Ingham (1983)	20	Panikker & Lavan (1975)	500
Jackson (1987)	50	Lin, Pepper & Lee (1976)	200
		Ta Phuoc Loc (1980)	1000
		Ecer, Rout & Ward (1983)	200
		Ta Phuoc Loc & Bouard (1985)	9500
		Braza, Chassaing & Ha Minh (1986)	1000
		Eaton (1987)	110

TABLE 1. Some of the existing literature on non-spectral numerical investigations of vortex shedding past cylinders

has already been used by Giorgini & Travis (1969), Travis & Giorgini (1971) and Orszag (1971), and in relation to the flow around a circular cylinder by Underwood (1969), Dennis & Chang (1970), Collins & Dennis (1973), Nieuwstadt & Keller (1973), Patel (1976), Giorgini & Rinaldo (1982), Ece, Walker & Doligalski (1984), Badr & Dennis (1985), Pravia & Giorgini (1985), and Avci & Giorgini (1985).

The present study deals with the numerical simulation of the non-symmetric non-steady flow of a viscous incompressible fluid past a circular cylinder at Reynolds number 1000 (based on the cylinder diameter), in which this kind of technique is used. The numerical laboratory used in this study, developed by Giorgini, Rinaldo and Pravia, is based on a mixed spectral–finite analytic numerical scheme (Giorgini & Rinaldo 1982 and Pravia & Giorgini 1985) whose main feature is the Fourier series expansion of the fields in the azimuthal direction which, for computational purposes, is approximated by the discrete Fourier transform and is carried out by a vectorized fast-Fourier-transform algorithm. The calculations have been executed with the CDC-CYBER 205 supercomputer of the Purdue University Computing Center. The graphical representations of the flow fields have been generated by using proprietary graphical codes developed by Giorgini, Rinaldo and Pravia (figures 4, 8, 9, 10, 11). The time advancement is performed by means of both a fourth-order Runge–Kutta scheme and a fourth-order predictor-corrector algorithm, in which the Adam–Moulton formula is implemented; fourth-order Newton–Cotes solutions are used in the radial direction. The main characteristics of the model are summarized in §§2 and 3. In order that the process of simulation behave in a non-symmetric fashion, an initial perturbation, consisting of a small rotational field, is introduced at the non-dimensional time $t = 0$. The detailed description of the perturbation vortex is given in §4 and the results are reported and discussed in §§5 and 6.

This research was performed for two main reasons. (i) To investigate the influence of an initial perturbation on the vortex shedding past a circular cylinder, given the fact that the nature of the corresponding physical phenomenon is derived from the

presence of perturbing instabilities, causing the asymmetric configuration of the wake past the cylinder. (ii) To obtain new insights into the fundamental mechanisms governing the formation of the near wake, by monitoring over time the evolution of the calculated flow fields. Sections 2 and 3 are summaries of the unpublished report by Pravia & Giorgini (1985).

2. Mathematical formulation (Pravia & Giorgini 1985)

The governing equations for the time-dependent two-dimensional flow of a viscous incompressible fluid, with no body forces and constant properties (the momentum conservation equations or Navier–Stokes equations), and the continuity equation, together with the definitions of stream function ψ and vorticity ζ, are considered. By eliminating the pressure and substituting the aforementioned definitions, one obtains the elliptic Poisson equation

$$\nabla^2\psi = \zeta \tag{1}$$

and the vorticity transport equation

$$\frac{\partial\zeta}{\partial t}+\frac{\partial\psi}{\partial y}\frac{\partial\zeta}{\partial x}-\frac{\partial\psi}{\partial x}\frac{\partial\zeta}{\partial y} = \nu\nabla^2\zeta, \tag{2}$$

in which the following non-dimensional groups have been introduced:

$$x=\frac{\hat{x}}{R};\quad y=\frac{\hat{y}}{R};\quad t=\frac{\hat{t}U}{R};\quad \psi=\frac{\hat{\psi}}{RU};\quad \zeta=\frac{\hat{\zeta}R}{U};\quad \nu=\frac{1}{Re}=\frac{\hat{\nu}}{UR};$$

R is the cylinder radius, U is the free-stream velocity and $\hat{\nu}$ the kinematic viscosity. The polar coordinate system is introduced, yielding

$$\frac{\partial\zeta}{\partial t}-\frac{1}{r}\left(\frac{\partial\psi}{\partial r}\frac{\partial\zeta}{\partial\theta}-\frac{\partial\psi}{\partial\theta}\frac{\partial\zeta}{\partial r}\right) = \nu\nabla^2\zeta, \tag{3}$$

while (1) is formally not affected, except that

$$\nabla^2 = \frac{\partial^2}{\partial r^2}+\frac{1}{r}\frac{\partial}{\partial r}+\frac{1}{r^2}\frac{\partial^2}{\partial\theta^2}.$$

The boundary conditions are no slip at the wall and free-stream velocity at infinity. The coordinate system is then modified by substituting the radial elongation with its logarithm (see also Son & Hanratty 1969; Dennis & Chang 1970; Fornberg 1980, among others). By also transforming the previous equations into a perturbed form, representing the difference between the actual flow and the uniform one (formally $\psi = \psi + e^{\xi}\sin\theta$), the Navier–Stokes equations become

$$e^{2\xi}\frac{\partial\zeta}{\partial t}+\frac{\partial\psi}{\partial\theta}\frac{\partial\zeta}{\partial\xi}-\frac{\partial\psi}{\partial\xi}\frac{\partial\zeta}{\partial\theta}+e^{\xi}\left(\cos\theta\frac{\partial\zeta}{\partial\xi}-\sin\theta\frac{\partial\zeta}{\partial\theta}\right)-\frac{1}{Re}\left(\frac{\partial^2\zeta}{\partial\xi^2}+\frac{\partial^2\zeta}{\partial\theta^2}\right) = 0, \tag{4}$$

and the boundary conditions become

$$\psi(0) = \left.\frac{\partial \psi}{\partial \xi}\right|_{\xi=0} = -\sin\theta, \tag{5}$$

$$\psi(\infty) = \left.\frac{\partial \psi}{\partial \xi}\right|_{\xi=\infty} = 0, \tag{6}$$

whereas the vorticity is unaffected. The fields are expanded in Fourier series along the azimuthal coordinate, as

$$\psi(\xi,\theta,t) = \sum_{\kappa=-\infty}^{\infty} \psi_\kappa(\xi,t)\,\mathrm{e}^{\mathrm{i}\kappa\theta}, \tag{7}$$

$$\zeta(\xi,\theta,t) = \sum_{\kappa=-\infty}^{\infty} \zeta_\kappa(\xi,t)\,\mathrm{e}^{\mathrm{i}\kappa\theta}. \tag{8}$$

By performing the appropriate substitutions, for any wave number κ, the following expressions are obtained:

$$\mathrm{e}^{2\xi}\frac{\partial \zeta_\kappa}{\partial t} + \mathrm{Conv}\,[\mathrm{i}\kappa\psi_\kappa \,|\, \zeta'_\kappa] - \mathrm{Conv}\,[\psi'_\kappa \,|\, \mathrm{i}\kappa\zeta_\kappa]$$

$$+\tfrac{1}{2}\mathrm{e}^{\xi}[\zeta'_{\kappa-1} + \zeta'_{\kappa+1} + (\kappa+1)\,\zeta_{\kappa+1} - (\kappa-1)\,\zeta_{\kappa-1}] - \frac{1}{Re}(\zeta''_\kappa \kappa - \kappa^2\zeta_\kappa) = 0, \tag{9}$$

$$\psi''_\kappa - \kappa^2\psi_\kappa = -\mathrm{e}^{2\xi}\zeta_\kappa, \tag{10}$$

with boundary conditions

$$\psi_1(0) = \psi'_1(0) = \tfrac{1}{2}\mathrm{i}, \tag{11}$$

$$\psi_{-1}(0) = \psi'_{-1}(0) = -\tfrac{1}{2}\mathrm{i}, \tag{12}$$

$$\psi_\kappa(0) = \psi'_\kappa(0) = 0 \quad \text{for} \quad \kappa^2 \neq 1, \tag{13}$$

$$\psi_\kappa(\infty) = \psi'_\kappa(\infty) = 0 \quad \text{for} \quad \kappa^2 \neq 1. \tag{14}$$

Equation (10) is solved by using the method of variation of coefficients (Hamidi & Giorgini 1985)

$$\psi_\kappa(\xi) = A_\kappa(\xi)\,\mathrm{e}^{\kappa\xi} + B_\kappa(\xi)\,\mathrm{e}^{-\kappa\xi}, \tag{15}$$

where

$$A'_\kappa(\xi)\,\mathrm{e}^{\kappa\xi} + B'_\kappa(\xi)\,\mathrm{e}^{-\kappa\xi} = 0 \tag{16}$$

and

$$A_\kappa(\xi) = -\frac{1}{2\kappa}\int_0^\xi \mathrm{e}^{(2-\kappa)s}\,\zeta_\kappa(s)\,\mathrm{d}s + \tfrac{1}{2}\mathrm{i}\,\delta_{1\kappa}, \tag{17}$$

$$B_\kappa(\xi) = \frac{1}{2\kappa}\int_0^\xi \mathrm{e}^{(2+\kappa)s}\,\zeta_\kappa(s)\,\mathrm{d}s. \tag{18}$$

As a result, the following integral conditions (first introduced by Dennis & Chang 1970) must be satisfied:

$$\int_0^\infty \mathrm{e}^{(2-\kappa)s}\zeta_\kappa(s)\,\mathrm{d}s = 0 \quad \text{for} \quad \kappa \neq 1, \tag{19}$$

$$\int_0^\infty \mathrm{e}^{(2+\kappa)s}\zeta_\kappa(s)\,\mathrm{d}s = \mathrm{i} \quad \text{for} \quad \kappa = 1. \tag{20}$$

The truncation of the infinite series of Fourier coefficients arising from the discretization of the space variable in the azimuthal direction is accomplished by

approximating the Fourier series with the discrete Fourier transform, which can be calculated by means of the fast-Fourier-transform algorithm (Cooley & Tukey 1965; Giorgini 1968) for the evaluation of the convolutions arising from the convective terms of the governing equations. The time advancement (except at the wall) is performed by two methods. At the initial four iterations a fourth-order Runge–Kutta solution is used; starting at the fifth iteration, a fourth-order predictor-corrector method is implemented, using the four values of the vorticity and of its time derivatives already calculated. In this case the Adam–Moulton formula is used, with coefficients taken from Crane & Klopfenstein (1965); the use of the predictor-corrector formula brings a remarkable saving in computer time (order of 60%), without consequences for the accuracy of the calculations. The time advancement of the vorticity field at the wall is obtained by enforcing (19) and (20) at the projected instant. Once the vorticity Fourier coefficients are obtained for each time step, the spatial derivatives are calculated by using fourth-order Newton–Cotes formulae. Skewed backward finite-difference schemes are used at the boundary points. Further information about the computer model can be found in Rinaldo & Giorgini (1984).

3. Reliability of the model (Pravia & Giorgini 1985)

To correctly portray the phenomenon to be simulated, the mesh size must be smaller than the spatial variation of the fields; the number of Fourier modes is an indicator of the refinement along the azimuthal coordinate, while in the radial direction the criterion used has been the one of keeping

$$\Delta\xi < \tfrac{2}{3}\delta^* = \tfrac{4}{3}(Re^*)^{-\frac{1}{2}}, \tag{21}$$

where δ^* is the non-dimensional Hiemenz solution for the boundary-layer thickness at the upstream stagnation point of a circular cylinder and Re^* is the Reynolds number based on the cylinder radius. While the upper-bound value of $\Delta\xi$ affects the correct representation of the phenomenon, the corresponding upper bound of Δt affects the stability of the calculations. Roache (1976) found that a stable relation between $\Delta\xi$ and Δt is in the form

$$\Delta t = \frac{\Delta\xi^2}{2\gamma}, \tag{22}$$

which has been found valid for values of $(1/\gamma) < 41.5$; accordingly, the criterion

$$\Delta t < 20\Delta\xi^2 \tag{23}$$

has been chosen which has been found to be stable for a Reynolds-number range of 20 to 50000 and a Fourier-series cutoff range of 16 to 256. Throughout the numerical experiments, the radial grid size was $\pi/64$ and the non-dimensional time increment was varied between 0.025 and 0.005.

In dealing with an unsteady flow, the perturbation caused by the presence of the cylinder propagates radially from its surface, and accordingly the number of radial stations must be increased in time; this creates the need to determine whether the results of the calculations are inaccurate owing to the effect of the outer boundary and/or to observe early indications of numerical instabilities in the system. These purposes are accomplished by monitoring – at each time step of integration – the behaviour of two graphs. The first is a plot of the enstrophy function, on a logarithmic scale, against the radial position, on an arithmetic scale. The values of

$$\alpha = f(\xi) = \sum_{\kappa} \zeta_\kappa(\xi)\,\zeta_\kappa^*(\xi) \tag{24}$$

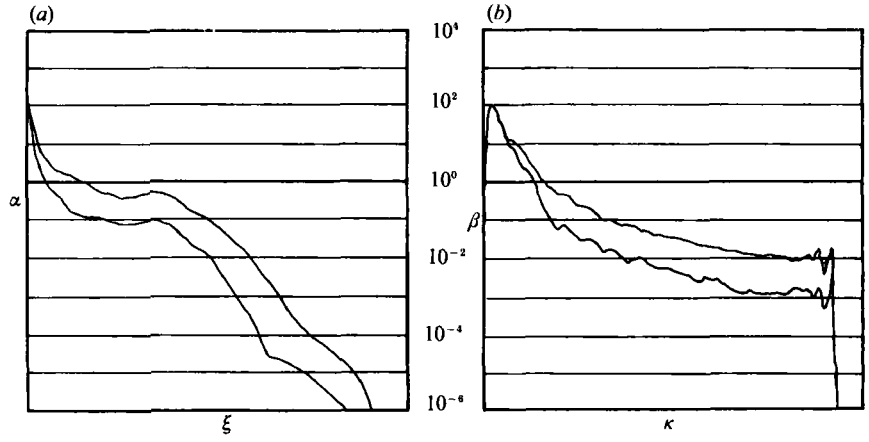

FIGURE 1. Typical diagnostic graphs.

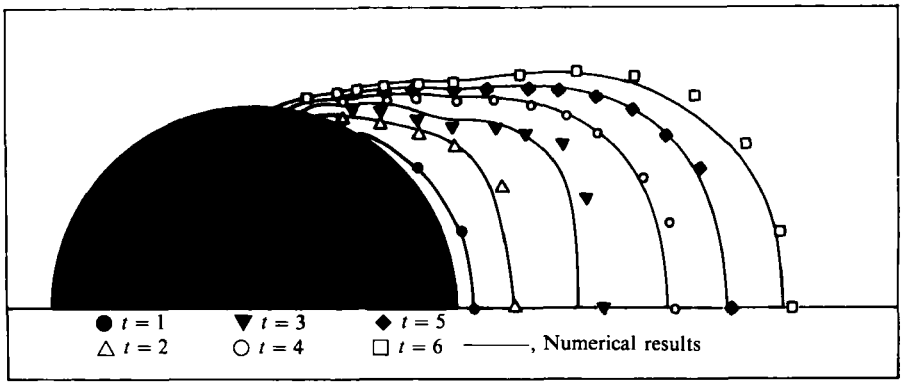

FIGURE 2. Comparison between experimental results due to Bouard & Coutanceau (1980) and numerical results obtained with the present model for the shape of the bubble wake ($Re = 3000$) (from Pravia & Giorgini 1985).

are calculated and plotted for each radial position (figure 1*a*). The upper curve represents the values just described, while the lower is the maximum single-mode value of α encountered for each radial position. The difference between the two curves represents the enstrophy stored in the rest of the modes, for each position ξ; the closer the curves are, the more reliable are the results. The criterion to determine the need for additional radial positions is the following: whenever the enstrophy at the outer boundary is of the order of 10^{-6}, the number of radial stations is increased (increments of 8 are used). Figure 1 (*b*) is a plot of the logarithm of the enstrophy with respect to the modes

$$\beta = f(\kappa) = \sum_{\xi} \zeta_{\kappa}(\xi)\, \zeta_{\kappa}^{*}(\xi); \tag{25}$$

here, too, the upper curve represents the sum of all the enstrophy in each mode along the radius, while the lower is the maximum single-station enstrophy for a given mode. It is expected that the enstrophy will decrease exponentially along the modes; in the graph the function should behave linearly. The criterion for increasing the

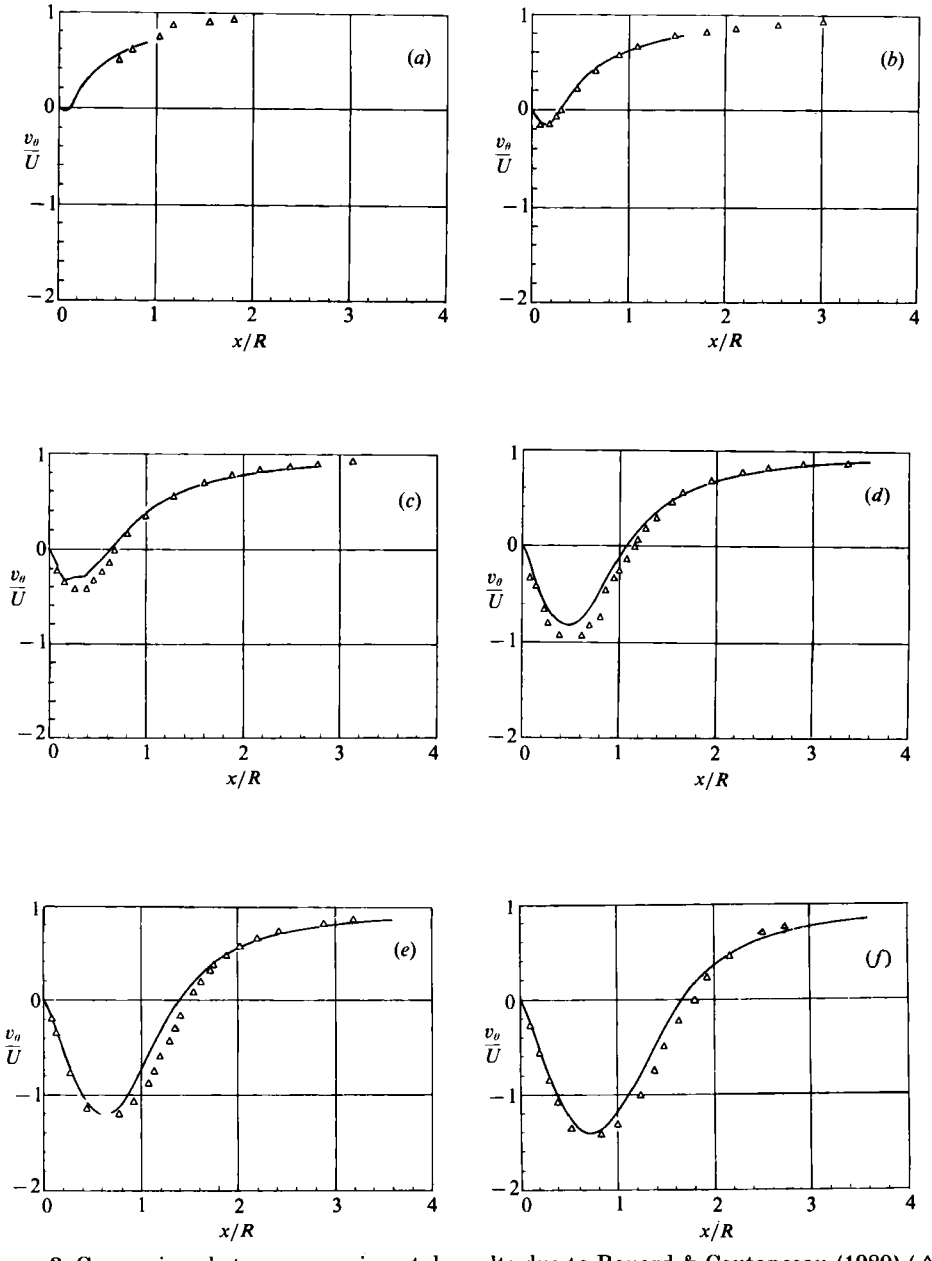

FIGURE 3. Comparison between experimental results due to Bouard & Coutanceau (1980) (△) and numerical results obtained with the present model (——) ($Re = 3000$), for the radial component of the velocity at $\theta = 0$; (*a*) $t = 1$, (*b*) $t = 2$, (*c*) $t = 3$, (*d*) $t = 4$, (*e*) $t = 5$, (*f*) $t = 6$ (from Pravia & Giorgini 1985).

number of modes has been established as follows: whenever the highest modes are four orders of magnitude less than the first one, then the number of modes is doubled. Accordingly, the number for the Fourier series cutoff has been varied from 16 to 64. The number of radial positions has been varied from 20 to 92.

The aim of this work is to give new insights into both the characteristics of the near

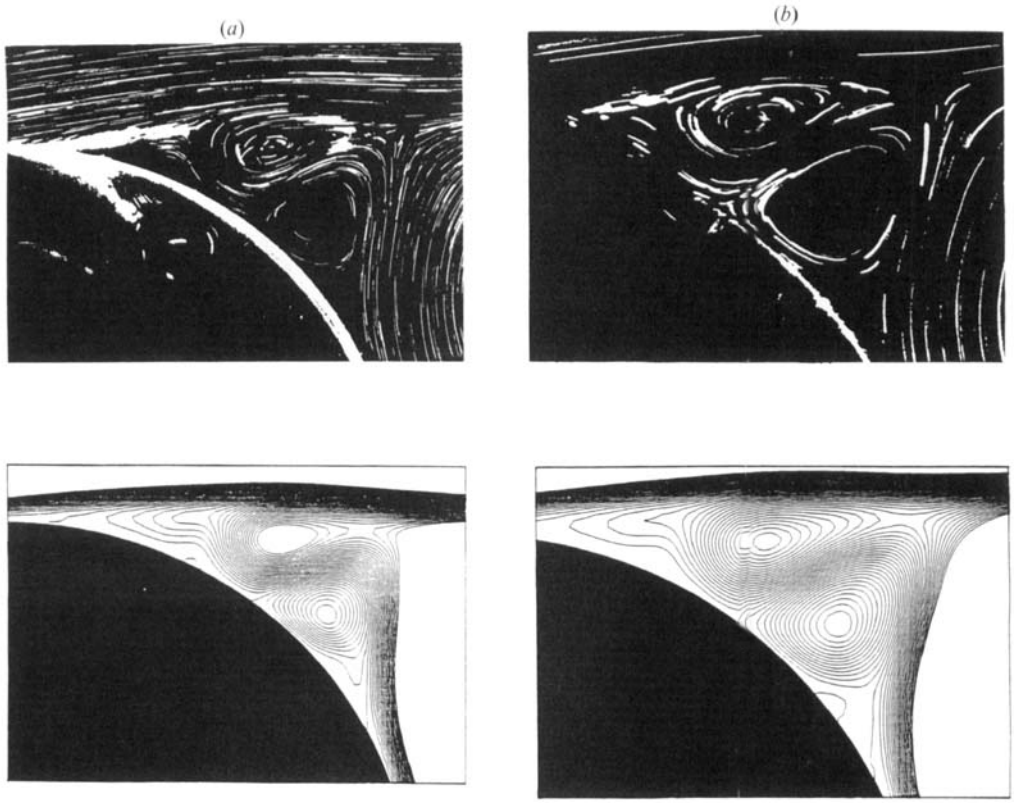

FIGURE 4. Comparison between flow visualizations of secondary vortices at the cylinder wall due to M. Coutanceau (1985, private communication) (top) and streamline representations obtained with the present model ($Re = 3000$) (bottom); (*a*) $t = 4$, (*b*) $t = 5$.

wake and the effect of a change of the initial conditions for non-steady non-symmetric flow past a circular cylinder, by performing numerical simulations with the mathematical model described above. This technique is referred in the literature as a numerical experiment in fluid mechanics (Aref 1986) and becomes of particular relevance in cases that are not easy to investigate with experimental techniques. In order to test the accuracy of the model against other results, some comparisons have been performed by the authors of the model; in figures 2 and 3(*a–f*) experimental results obtained by Bouard & Coutanceau (1980) for the shape of the wake and related radial velocities at different instants at $Re = 3000$, are compared with numerical results obtained with this model. In figures 4(*a*) and 4(*b*) photographs of flow visualizations at $Re = 3000$ (M. Coutanceau 1985, private communication) are compared with streamlines of secondary vortices obtained with this model. In figures 5(*a*), 5(*b*) and 5(*c*) comparisons between numerical results due to Braza *et al.* (1986) for the distribution of vorticity at the wall at different instants for non-steady non-symmetric flow past a circular cylinder at $Re = 1000$ are compared with the present work. The differences noticeable in the lower parts of the graphs at $t = 2$ and $t = 3$ are a consequence of the different nature of the perturbations used in the two works. Other comparisons concerning the length of the bubble wake, the evolution of the separation angles, steady-state vorticity and pressure distribution at the wall have

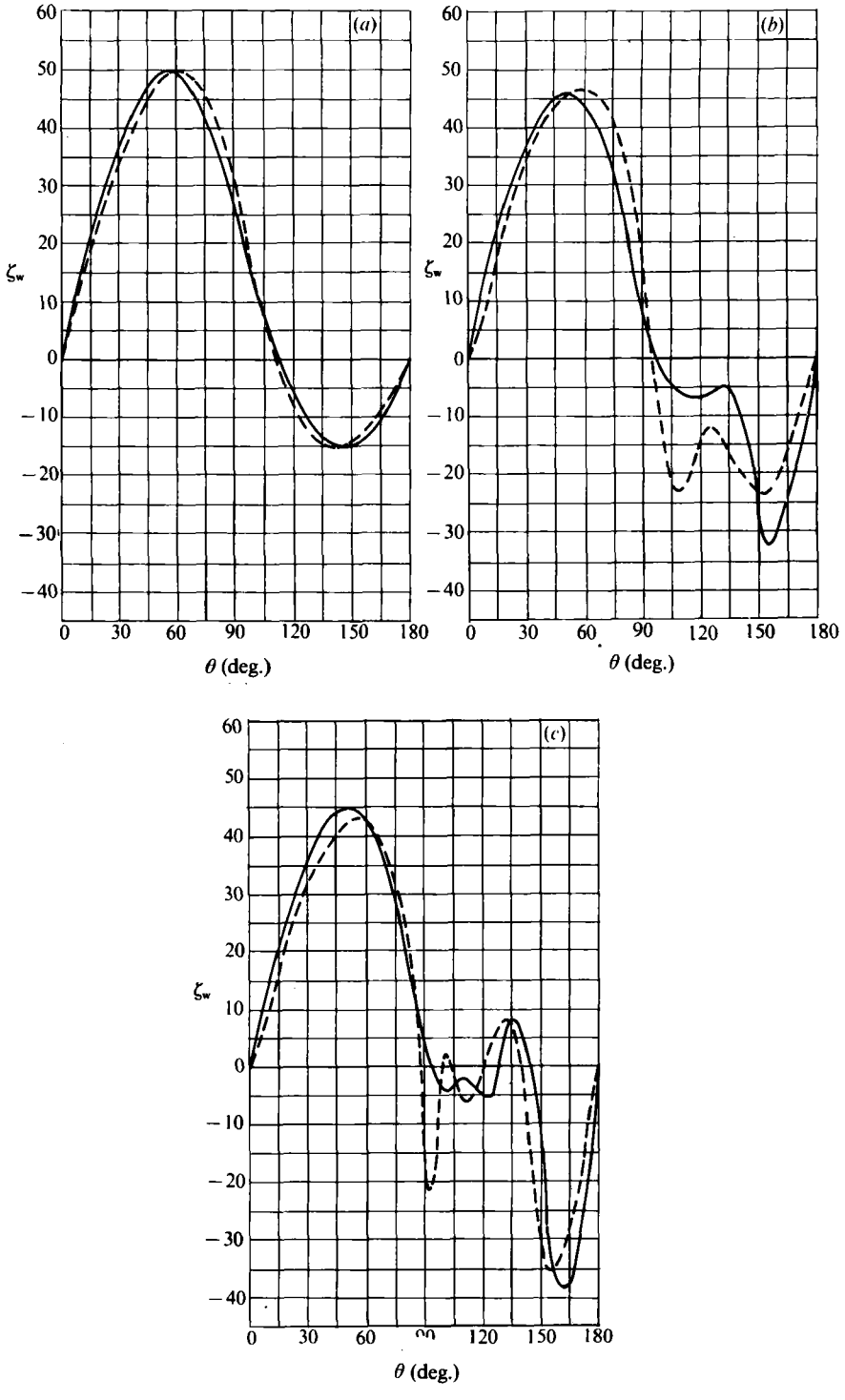

FIGURE 5. Comparison between numerical results due to Braza *et al.* (1986) (– – –) and the present work (——) for the distribution of vorticity at the cylinder wall ($Re = 1000$); (*a*) $t = 1$, (*b*) $t = 2$, (*c*) $t = 3$.

Experiment	C	S	n	σ	$(v_\theta)_{\max}$
0.2/10	0.2	0.2/56	10	2/7	0.008
0.4/10	0.4	0.4/56	10	2/7	0.015
0.8/10	0.8	0.8/56	10	2/7	0.031
1.6/10	1.6	1.6/56	10	2/7	0.062

TABLE 2. Parameters characterizing the perturbation vortices

already been shown in a previous paper (Rinaldo & Giorgini 1984), where this model was first presented.

4. The perturbation vortex

Several ways have been devised in different numerical studies to perturb the flow fields in order to simulate the non-symmetric configuration of the wake downstream of a cylinder. In some of them the cylinder translates and rotates simultaneously (Ece *et al.* 1984; Badr & Dennis 1985), while in others the cylindrical body initially rotates (Jordan & Fromm 1972; Braza *et al.* 1986). In this study the initial perturbation is a small rotational field, imposed at the non-dimensional time $t = 0$ to the initially irrotational flow. By assuming the following two-parameter mathematical formulation for the function representing the azimuthal velocity:

$$v_\theta = \frac{C}{r^n}(r-1) = C\left(\frac{1}{r^{(n-1)}} - \frac{1}{r^n}\right), \tag{26}$$

and considering an expression with the meaning of an angular momentum, one obtains

$$S = \int_1^\infty r v_\theta \, \mathrm{d}r = C\int_1^\infty \left(\frac{1}{r^{(n-2)}} - \frac{1}{r^{(n-1)}}\right)\mathrm{d}r = \frac{C}{(n-2)(n-3)}; \tag{27}$$

the quantity $C/(n-2)(n-3)$ becomes a measure of the strength of the perturbation vortex. Another attribute of the perturbation function is its spread, which can be defined as the distance from the cylinder wall where all the discharge should be placed in order to have the same moment; by considering the following expression:

$$D\int_1^\infty v_\theta \, \mathrm{d}r = \int_1^\infty r v_\theta \, \mathrm{d}r \tag{28}$$

one obtains the distance from the cylinder wall as

$$\sigma = D - 1 = \frac{2}{n-3}, \tag{29}$$

where D is the distance from the centre in units of the cylinder radius. In order to devise a range of variation for the two parameters C and n for different numerical experiments the following procedure has been followed: by choosing a value of n ($n = 10$), the corresponding value of σ is determined. By also choosing a set of values of C (0.2, 0.4, 0.8, 1.6, each one double the previous one) the corresponding values of

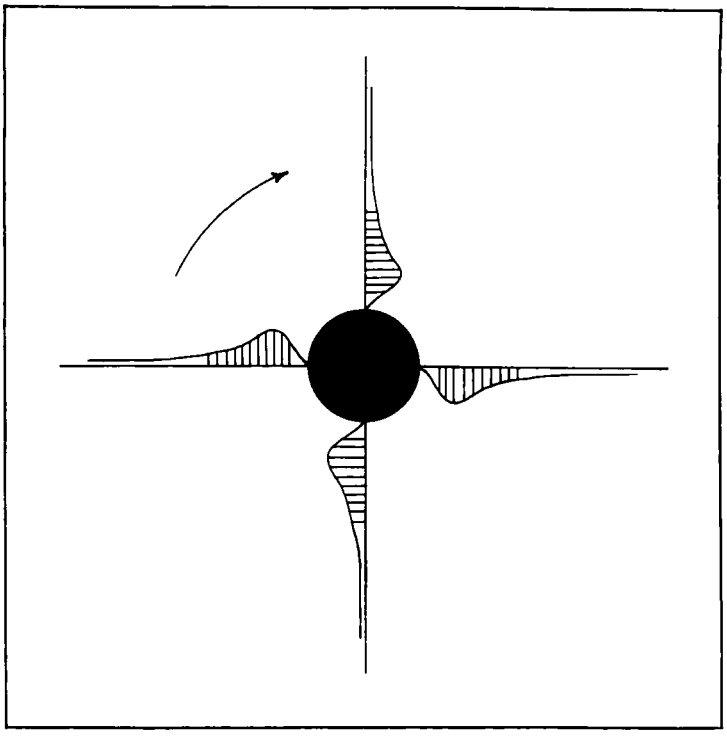

FIGURE 6. The perturbation vortex.

S are determined. In this way a group of four perturbations with constant spread and increasing strength (each value is the double of the previous one) is identified. The values of the parameters C and n characterizing the numerical simulations with respect to the perturbation, are reported in table 2. Also, in this table the values of the function

$$(v_\theta)_{\max} = \frac{C}{n}\left(\frac{n-1}{n}\right)^{n-1} \tag{30}$$

are reported in terms of C. It can be noticed that $(v_\theta)_{\max}$ reaches at most 6.2% of the free-stream velocity, in the experiment characterized by the highest perturbation strength.

Figure 6 shows a qualitative representation of the perturbation vortex.

5. Numerical experiments

The numerical experiments will be identified by the kind of perturbation imposed at $t = 0$, which will be indicated by the two numbers representing the values of the parameters C and n in their mathematical formulation (table 2); the results of the simulations are illustrated by three different flow-field representations: absolute streamlines, relative streamlines (relative to an observer travelling with the cylinder) and vorticity field. For both the absolute and relative streamlines, the interstreamline interval is 0.1 and the thick line has the stream-function value $\psi = 0$; in the absolute

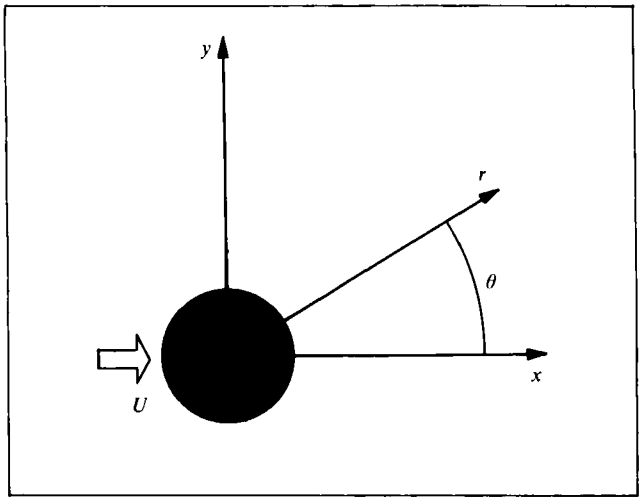

FIGURE 7. The system of coordinates.

t	N	K	Δt	t	N	K	Δt
1	20	16	0.0250	11–12	52	64	0.0080
2	28	16	0.0250	13–16	60	64	0.0080
3	28	32	0.0250	17–22	68	64	0.0080
4	36	32	0.0250	23–28	76	64	0.0080
5	36	64	0.0125	29–35	84	64	0.0080
6–9	44	64	0.0125	36–40	92	64	0.0050
10	52	64	0.0125				

TABLE 3. Computational parameters

streamlines, the lines containing saddle points are also thick. The vorticity threshold between the black areas and the rest of the field is $(2Re)^{\frac{1}{2}}/20$. The vortices have been numbered according to the order in which they detach from the cylinder and given a letter, U (upper) or L (lower), depending on whether the vortex has formed in the upper or in the lower part of the field, with respect to the x-axis (figure 7). The experiments have been conducted with the values of radial position N, Fourier mode K and Δt shown in table 3 (see also Alfonsi 1988; Alfonsi & Giorgini 1987).

5.1. *Experiment* 0.2/10

By $t = 16$ (figure 8a) the asymmetry in the flow field is already evident; vortex U_2 is an α-vortex while vortex L_1 is a D vortex. (The terms α-vortex and D-vortex have the following meaning: free or detached vortices are encircled by a streamline that intersects itself, creating a figure which resembles the lower-case Greek letter α; attached vortices are entirely encircled by the wall and by a streamline which starts at a point of the wall and ends at another point of the wall, creating a figure which resembles the upper case Latin letter D.) According to the absolute streamlines, vortex U_2 starts moving away from the cylinder wall and this process is clearly

visible until $t = 22$ (figure 8*b*); then it moves backward and by $t = 26$ (figure 8*c*) is attached again. During this 'temporary detachment', vortex L_1 starts growing markedly, and by $t = 26$ is detached and starts travelling downstream. At this instant, the U_2 vorticity area is considerably more elongated than the L_1, which has assumed a rounded shape. At $t = 28$ (figure 8*d*) the elongation of the U_2 vorticity area becomes more pronounced and by $t = 30$ it has lost its tail, which keeps moving (figure 8*e*); vortex U_2 has broken into two parts as a consequence of the upward movement of vortex L_1 (relative streamlines). Its main part becomes rounded and this new shape is in good agreement with the picture given by the absolute streamlines, from which it can be seen that vortex U_2 has just detached and is also rounded. Although vortex L_1 looks already separated on the basis of the absolute streamlines, its vorticity area is still connected to the cylinder and will separate later, when an independent vorticity lump will form. By $t = 32$ (figure 8*f*) vortex L_1 is not visible anymore in the way it was familiar before, but a sudden change in the direction of the streamlines is noticeable, revealing the existence of a vorticity sheet, which keeps travelling downstream until a vorticity lump appears. A new vortex – L_3 – also becomes evident and vortex U_4 appears by $t = 36$ (figure 8*g*).

5.2. *Experiment* 0.4/10

In this case the first vortex to detach is in the upper part of the field (U_1) and the second in the lower (L_2); there is a tendency of the L_2 vorticity area to assume an elongated shape and, at the same time, of the U_1 vorticity area to have a rounded one. The absolute streamlines show that by $t = 16$ (figure 9*a*) vortex L_2 is a *D* vortex (attached to the cylinder), and U_1 is detached and starts travelling downstream. By $t = 20$ (figure 9*b*) the U_1 vorticity area overcomes the L_2 one, which starts assuming a rounded shape; this is related to the process of detachment of vortex U_1 (see the absolute streamlines) which determines the extent of the vorticity area in the region of its movement. This process is similar to that observed in the previous experiment (0.2/10) and called there temporary detachment, the only difference being that now vortex U_1 shows a permanent detachment. Vortex L_2 keeps growing, separates by $t = 24$ and starts travelling downstream (figure 9*c*). Its growth is also clearly visible in the relative streamlines and in the vorticity field, from which it can be noticed how the upward movement of the L_2 vorticity area contributes to the breakup of the U_1 vorticity area; by $t = 28$ both U_1 and L_2 have developed in independent vorticity lumps (figure 9*d*) while vortex U_3 has appeared and separates, according to the absolute streamlines.

5.3. *Experiment* 0.8/10

By $t = 14$ (figure 10*a*) vortex L_2 has just separated from the cylinder and vortex U_1, attached to the cylinder, grows markedly; during this temporary detachment phase the L_2 vorticity area is still elongated while the U_1 starts growing, according to what can be seen in the streamlines. By $t = 16$ (figure 10*b*) vortex U_1 is detached from the cylinder and has reached remarkable dimensions; vortex L_2 is attached and is smaller than in the previous instants. Vortex U_1 starts travelling downstream and its vorticity area grows; by $t = 20$ in the area already occupied by vortex U_1 in the absolute streamlines, only a sudden change in the direction of the streamlines appears, while vortex L_2 has grown markedly. The vorticity field shows an elongation of U_1 and a tendency of L_2 to become rounded. The L_2 area starts pushing upward and contributes to the breakup of L_1 (relative streamlines). This phenomenon

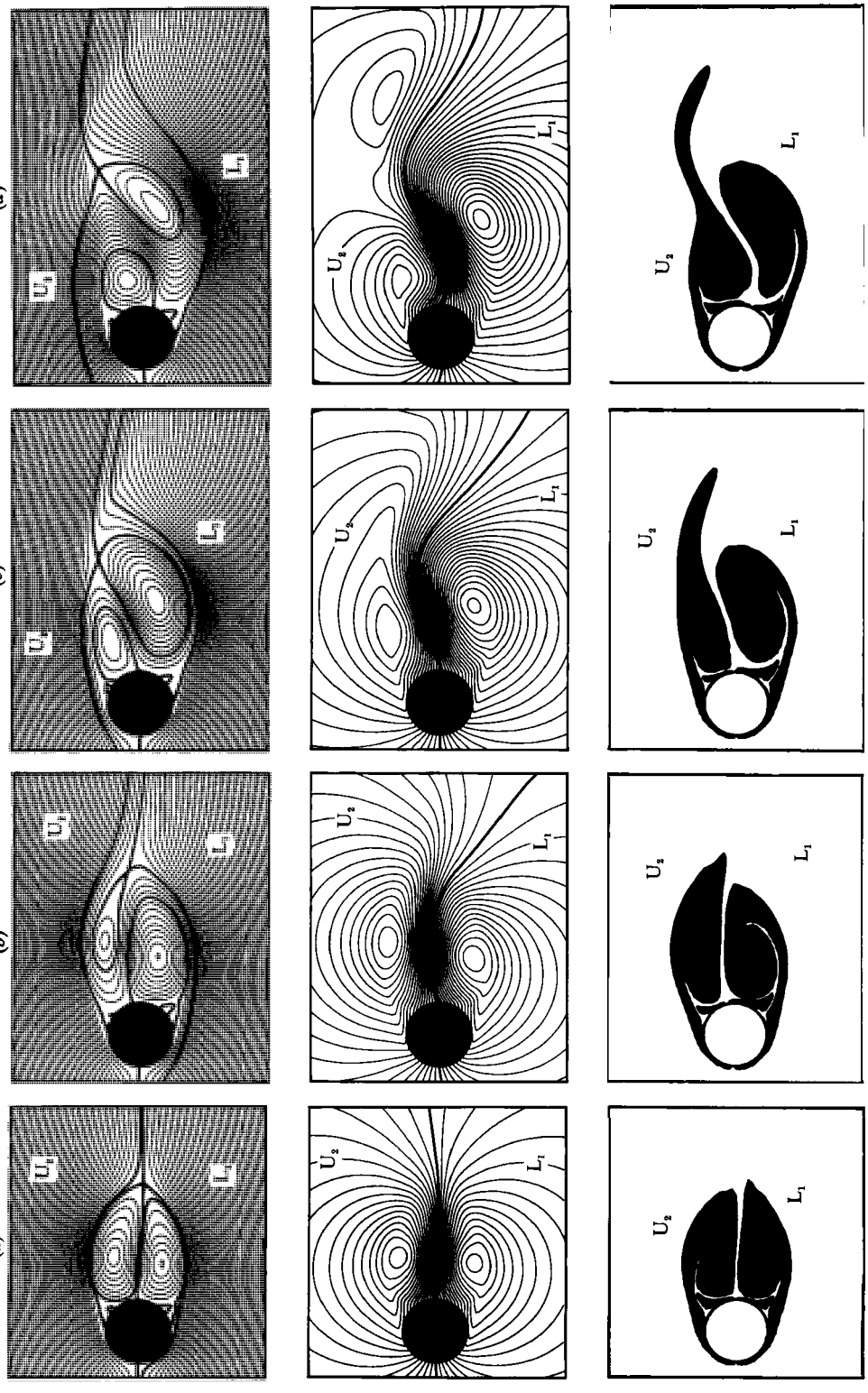
(a)
(b)
(c)
(d)
U1
U2
L1

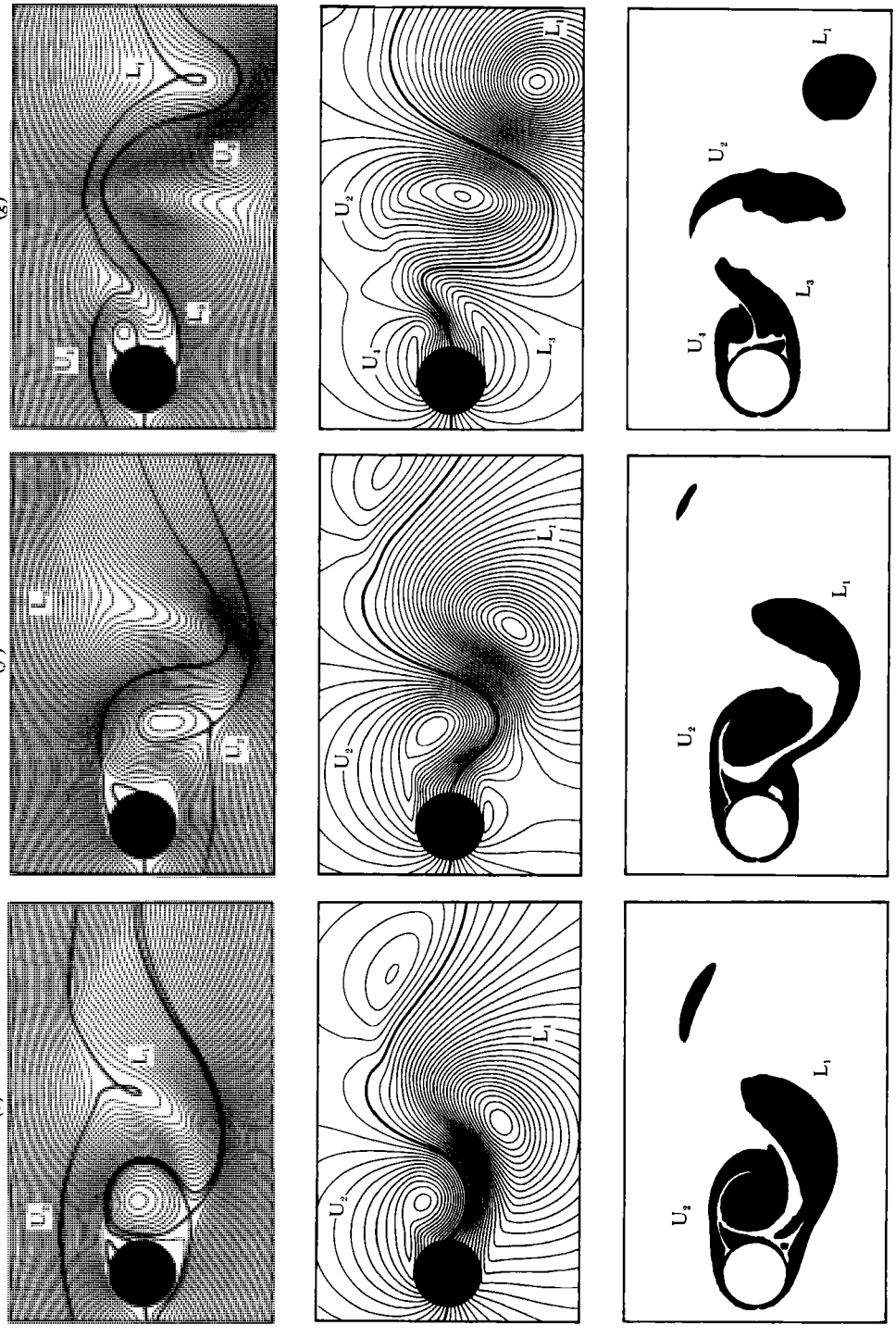

FIGURE 8. Experiment 0.2/10. Absolute streamlines, relative streamlines and vorticity field (from top to bottom) at (*a*) $t = 16$, (*b*) $t = 22$, (*c*) $t = 26$, (*d*) $t = 28$, (*e*) $t = 30$, (*f*) $t = 32$, (*g*) $t = 36$.

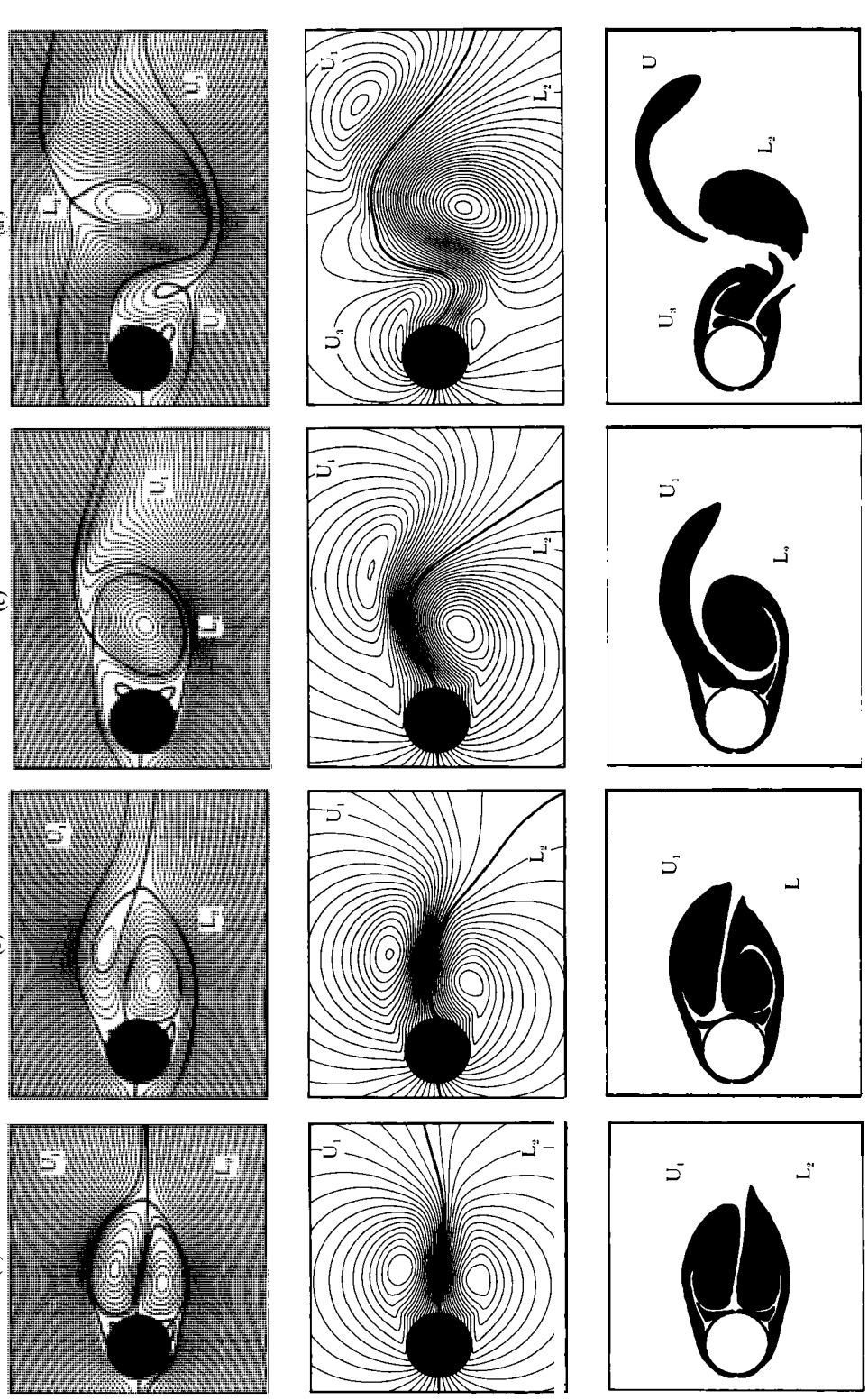

FIGURE 9. Experiment 0.4/40. Absolute streamlines, relative streamlines and vorticity field (from top to bottom) at: (*a*) $t = 146$, (*b*) $t = 200$, (*c*) $t = 244$, (*d*) $t = 288$.

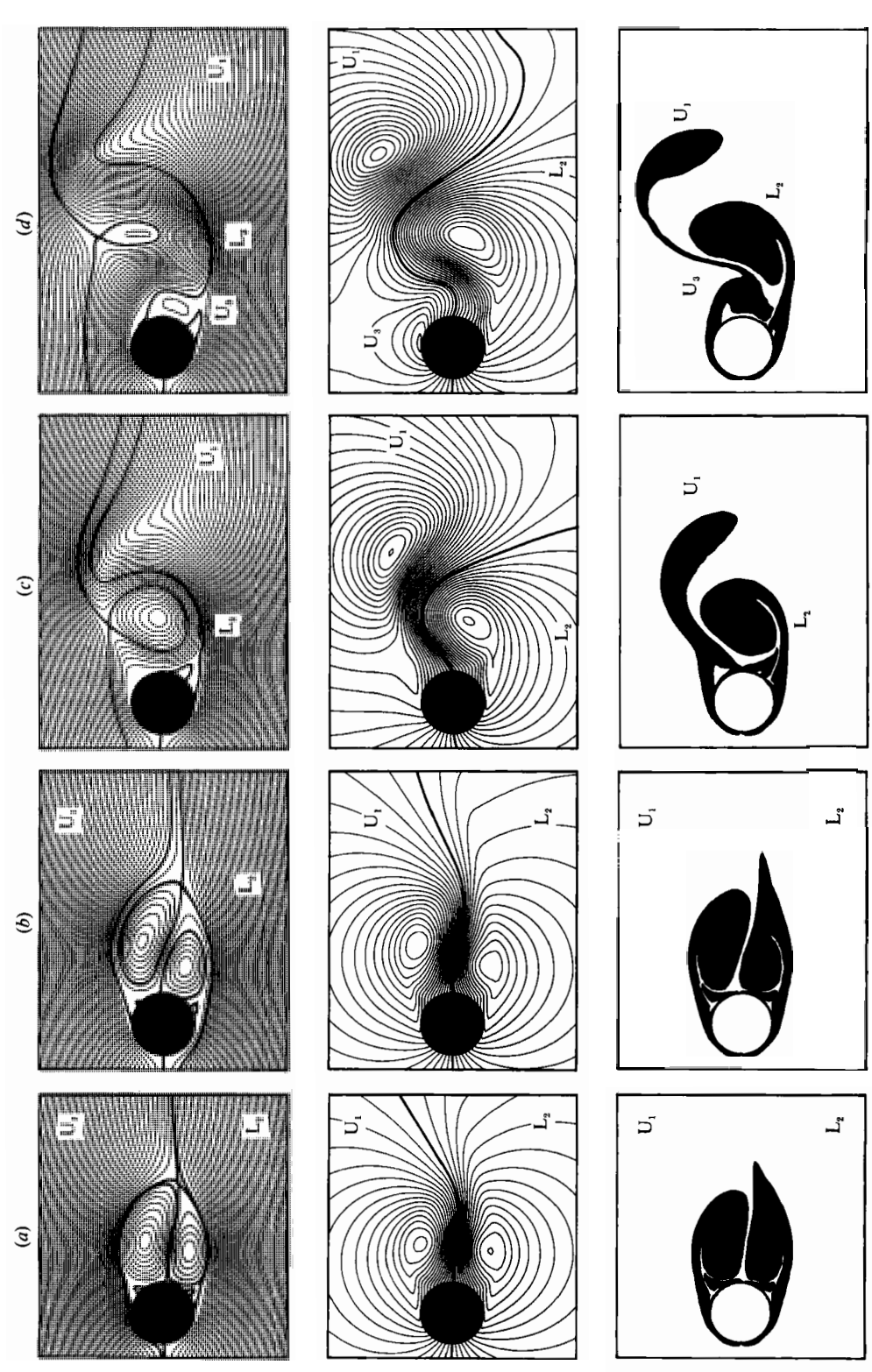

FIGURE 10. Experiment 0.8/10. Absolute streamlines, relative streamlines and vorticity field (from top to bottom) at (*a*) $t = 14$, (*b*) $t = 16$, (*c*) $t = 22$, (*d*) $t = 24$.

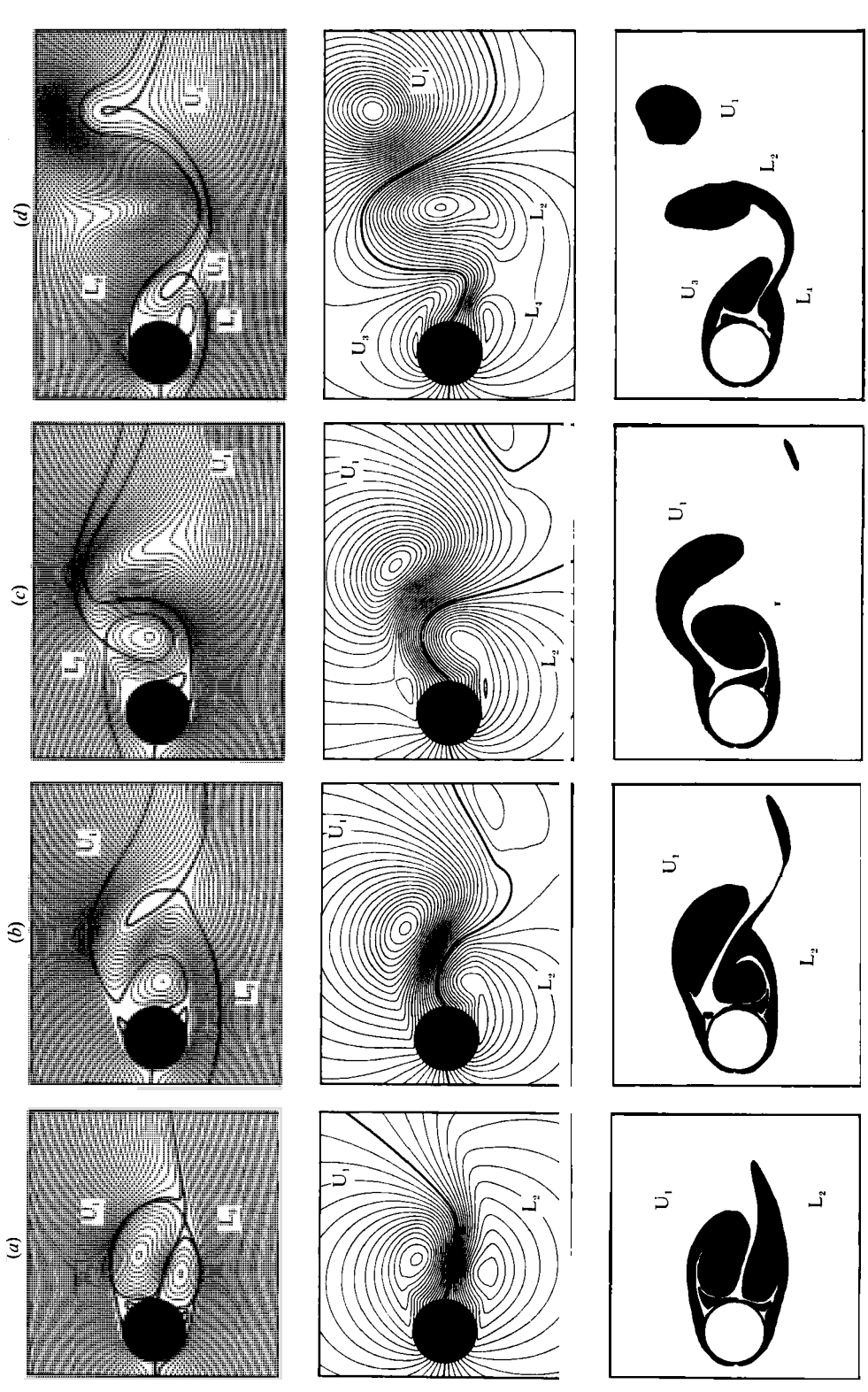

FIGURE 11. Experiment 1.6/10. Absolute streamlines, relative streamlines and vorticity field (from top to bottom) at (*a*) $t = 14$, (*b*) $t = 18$, (*c*) $t = 20$, (*d*) $t = 24$.

Experiment	S	σ	First detached vortex
0.2/10	0.2/56	2/7	Lower
0.4/10	0.4/56	2/7	Upper
0.8/10	0.8/56	2/7	Upper
1.6/10	1.6/56	2/7	Upper

TABLE 4. First vortex to detach in each experiment

Exp. 0.2/10	L_1, U_2	Downward
Exp. 0.4/10	U_1	Upward
	L_2, U_3, L_4	Downward
Exp. 0.8/10	U_1, L_2	Upward
	U_3, L_4	Downward
Exp. 1.6/10	U_1, L_2, U_3	Upward
	L_4	Downward

TABLE 5. Characteristics of the movement of the vorticity lumps

develops through instants $t = 22$ (figure 10*c*) and $t = 24$ (when vortex U_3 appears, figure 10*d*) and by $t = 26$ the U_1 vorticity area becomes independent.

5.4. *Experiment* 1.6/10

By $t = 14$ (figure 11*a*) vortex L_2 is attached to the cylinder, while vortex U_1 has grown and is almost separated; by $t = 18$ (figure 11*b*) the L_2 vorticity area is about to lose its tail, while its main body is still close to the cylinder wall. At $t = 20$ the process is completed (figure 11*c*), vortex L_2 has also separated (absolute streamlines), the L_2 vorticity area has assumed a rounded shape and starts moving upward. By $t = 24$ U_1 is an independent vorticity lump and the elongation of the U_3 vorticity area is breaking up L_2 with the appearance of vortex L_4 (figure 11*d*, also from the relative streamlines).

6. Concluding remarks

All the different representations of the flow fields provide information that is often complementary, in the sense that whenever one of them becomes obscure or insufficient, another one takes its place and provides continuity to the description.

The onset of the development of the flow field is not the same for all the experiments with respect to the location (whether upper or lower) of the first vortex to separate, which determines the subsequent order of detachment for all the other vortices (table 4).

The strength of the initial perturbation influences the number of vortices observed at every instant that has been calculated, and, as a consequence, the total number of vortices observed at the end of each experiment. All the experiments show two vortices until $t = 21$ and then their number increases at higher rate in the experiments with the largest perturbation strength.

Another feature to be pointed out is the movement of the vorticity lumps once

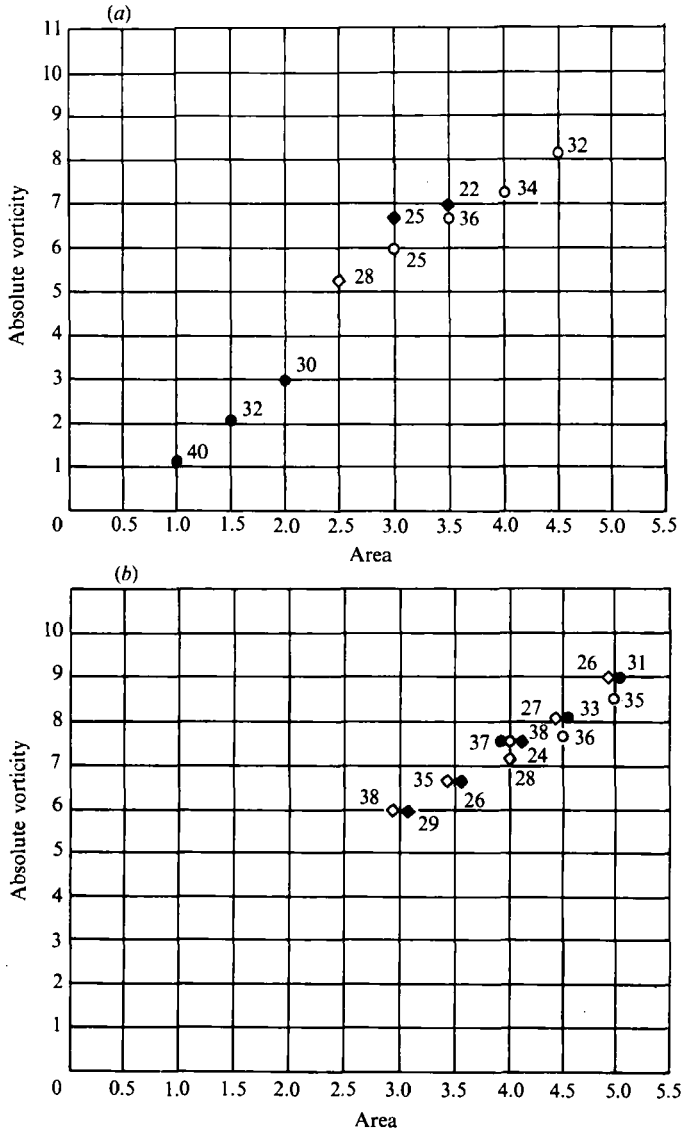

FIGURE 12. For caption see facing page.

they have become independent (table 5). Some further calculations have shown that, as time elapses, there is a tendency for the lumps to stay on the centreline. Moreover, concerning the behaviour of the first lump – and, as a consequence, of all the subsequent ones – it can be seen that, whenever the first vortex to separate is a lower one, its vorticity lump moves downward (experiment 0.2/10), while when the first vortex is an upper one, its lump moves upward.

In order to further investigate the evolution of the vorticity in the lumps, some additional graphs are reported; they portray the absolute vorticity – the integral of the vorticity field over the area of each lump – versus the area of the lumps, for each vortex in all the experiments. For vortex 1 (figure 12*a*) the values are quite

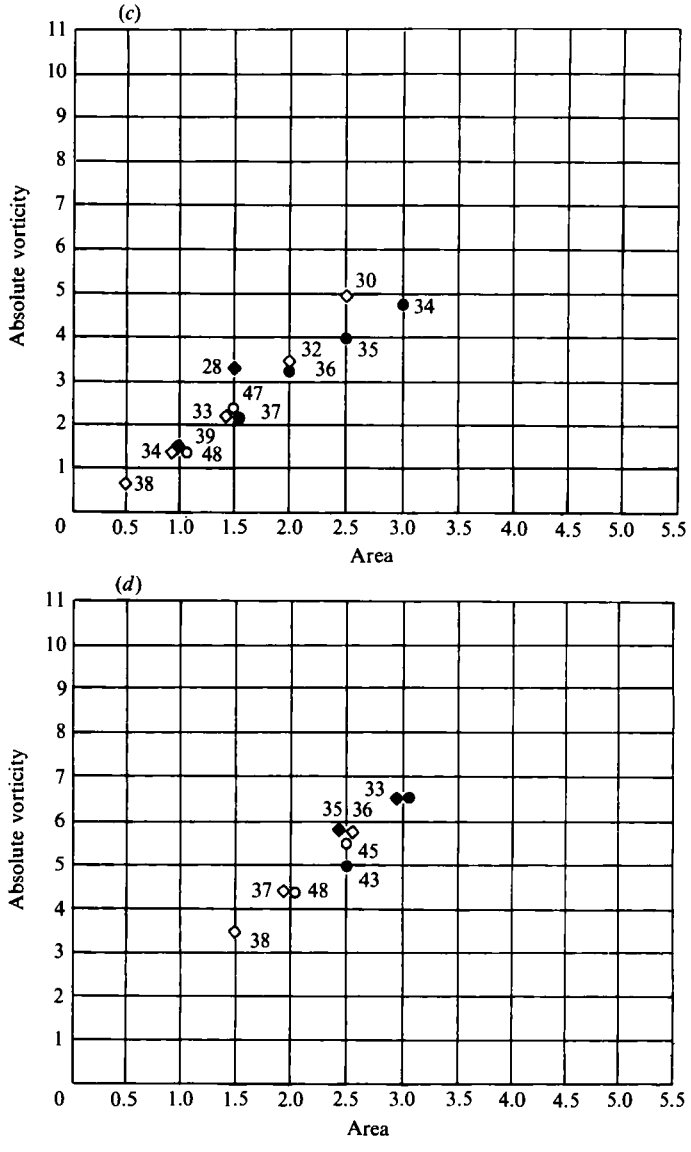

FIGURE 12. Absolute vorticity versus area: (*a*) vortex 1, (*b*) vortex 2, (*c*) vortex 3, (*d*) vortex 4. ○, Experiment 0.2/10; ●, 0.4/10; ◇, 0.8/10; ◆, 1.6/10. The number near each symbol is the non-dimensional time.

distributed; the highest values of absolute vorticity correspond to the largest vortex areas (experiment 0.2/10) and the lowest to the smallest areas (experiment 0.4/10). At the areas of 3.0 and 3.5 the absolute vorticity in experiment 1.6/10 is higher than for experiments 0.8/10 and 0.2/10. The equivalent graph for vortex 2 (figure 12*b*) shows some of the points grouped around the same values; the absolute vorticity in experiments 0.4/10 and 0.8/10 is higher than in experiment 0.2/10, for values of the area of 4.5 and 5.0. Then the vorticities of experiments 0.2/10, 0.4/10 and 1.6/10 become higher than those of 0.8/10 (area equal to 4.0) and finally the same values are

shown for experiments 0.8/10 and 1.6/10 at the area values 3.5 and 3.0. The points related to vortex 3 (figure 12*c*) are mainly concentrated in the small area values: several points are grouped around the areas 1.0 and 1.5. The absolute vorticities in experiment 0.8/10 are higher than in experiment 0.4/10 in the points towards the right. The points related to vortex 4 (figure 12*d*) are mainly concentrated in the central region of the graph and several of them are grouped around the area 2.5.

In §1 two reasons have been indicated for this study to be performed. The following conclusions can be drawn concerning the influence of the initial perturbation on the vortex shedding phenomenon.

(i) The increase in strength of the initial perturbation acts in such a way as to allow the vortices to detach earlier. As a consequence the number of vortices every instant and the total number of vortices observed at the end of each experiment are increased.

(ii) The strength of the initial perturbation does not directly influence the movement of the independent vorticity lumps, which is more closely related to the first vortex that separates.

(iii) The values of the total vorticity within the vorticity lumps are independent of the initial perturbation.

(iv) The step increase of the perturbation amplitude (each new value is double the previous one) was sufficient to generate four distinct experiments, each one with a different behaviour.

(v) A slight change in the characteristics of the initial condition has caused the first numerical experiment to be different from the other three of a similar nature in that, in the last three experiments, the first vortex to separate was an upper one, while in the first, it was a lower one.

New information has been obtained on the mechanisms governing the formation of the near wake, through the description of the temporal evolution of the computer-generated drawings of absolute streamlines, relative streamlines and vorticity fields.

Concerning the physical interpretation of these results, it should be kept in mind that the study has been conducted in two dimensions, while it is well known that at $Re = 1000$ three-dimensional effects are present. On the other hand such an approach allows a particular feature to be isolated – the effect of a change of the initial conditions – while in other similar numerical studies often only one value of the initial perturbation is tested. Moreover, the analysis has been limited to the primary vortices, despite of the fact that the present model has also been able to predict secondary and tertiary vortex structures (Pravia & Giorgini 1985).

REFERENCES

Abernathy, F. H. & Kronauer, R. E. 1962 The formation of vortex streets. *J. Fluid Mech.* **13**, 1.

Alfonsi, G. 1988 Influence of finite amplitude perturbations on the vortex shedding past a circular cylinder. Ph.D. dissertation, Purdue University, Indiana.

Alfonsi, G. & Giorgini, A. 1987 Influence of perturbation amplitude on the wake behind a circular cylinder: numerical experiments at $Re = 1000$. *Technical Rep.* CE-HSE-87-7. School of Civil Engineering, Purdue University, West Lafayette, Indiana.

Allen, D. N. de G. & Southwell, R. V. 1955 Relaxation methods applied to determine the motion, in two dimensions, of a viscous fluid past a fixed cylinder. *Q. J. Mech. Appl. Maths* **8**, 129.

APELT, C. J. 1958 The steady flow of a viscous fluid past a circular cylinder at Reynolds numbers 40 and 44. *Aero. Res. Counc. R. and M.* 3175.

AREF, H. 1986 The numerical experiment in fluid mechanics. *J. Fluid Mech.* **173**, 15.

AVCI, C. & GIORGINI, A. 1985 Impulsively started flow past elliptic cylinders: a numerical study. *Tech. Rep.* CE-HSE-87-02. School of Civil Engineering, Purdue University, West Lafayette, Indiana.

BADR, H. M. & DENNIS, S. C. R. 1985 Time-dependent viscous flow past an impulsively started rotating and translating circular cylinder. *J. Fluid Mech.* **158**, 447.

BAIRSTOW, L., CAVE, B. M. & LANG, E. D. 1922 The two-dimensional slow motion of viscous fluids. *Proc. R. Soc. Lond.* A **100**, 394.

BAIRSTOW, L., CAVE, B. M. & LANG, E. D. 1923 The resistance of a cylinder moving in a viscous fluid. *Proc. R. Soc. Lond.* A **223**, 383.

BOUARD, R. & COUTANCEAU, M. 1980 The early stage of development of the wake behind an impulsively started cylinder for $40 < Re < 10^4$. *J. Fluid Mech.* **101**, 583.

BRAZA, M., CHASSAING, P. & HA MINH, H. 1986 Numerical study and physical analysis of the pressure and velocity fields in the near wake of a circular cylinder. *J. Fluid Mech.* **165**, 79.

COLLINS, W. M. & DENNIS, S. C. R. 1973 Flow past an impulsively started circular cylinder. *J. Fluid Mech.* **60**, 105.

COOLEY, J. W. & TUKEY, J. W. 1965 An algorithm for the machine calculations of the complex Fourier series. *Math. Comput.* **19**, 297.

COWLEY, S. J. 1983 Computer extension and analytic continuation of Blasius' expansion for impulsive flow past a circular cylinder. *J. Fluid Mech.* **135**, 389.

CRANE, R. L. & KLOPFENSTEIN, R. W. 1965 A predictor-corrector algorithm with an increased range of absolute stability. *J. Assoc. Comput. Machinery* **12**, 227.

DENNIS, S. C. R. & CHANG, G. Z. 1970 Numerical solutions for steady flow past a circular cylinder at Reynolds numbers up to 100. *J. Fluid Mech.* **42**, 471.

EATON, B. E. 1987 Analysis of laminar vortex shedding behind a circular cylinder by computer aided flow visualization. *J. Fluid Mech.* **180**, 117.

ECE, M. C., WALKER, J. D. A. & DOLIGALSKI, T. L. 1984 The boundary layer on an impulsively started rotating and translating cylinder. *Phys. Fluids* **27**, 1077.

ECER, A., ROUT, R. K. & WARD, P. 1983 Investigation of solution of Navier–Stokes equations using a variational formulation. *Intl J. Numer. Meth. Fluids* **3**, 23.

FORNBERG, B. 1980 A numerical study of steady viscous flow past a circular cylinder. *J. Fluid Mech.* **98**, 819.

GIORGINI, A. 1968 Numerical Fourier analysis. *Tech. Rep.* 25. School of Civil Engineering, Purdue University, West Lafayette, Indiana.

GIORGINI, A. & ALFONSI, G. 1987 Influence of perturbation spread on the wake behind a circular cylinder: numerical experiments at $Re = 1000$. *Tech. Rep.* CE-HSE-87-8. School of Civil Engineering, Purdue University, West Lafayette, Indiana.

GIORGINI, A. & RINALDO, A. 1982 A mixed discrete Fourier transform–quasi analytic algorithm for the solution of the Navier–Stokes equations: presentation of the method. *Tech. Rep.* CE-HSE-82-17. School of Civil Engineering, Purdue University, West Lafayette, Indiana.

GIORGINI, A. & TRAVIS, J. R. 1969 A short convolution. *Tech. Rep.* 2. Water Resources and Hydromechanics Laboratory, School of Civil Engineering, Purdue University, West Lafayette, Indiana.

HAMIDI, A. & GIORGINI, A. 1985 Numerical solution of the Napier–Stokes equations: direct radial integration. *Tech. Rep.* CE-HSE-85-02. School of Civil Engineering, Purdue University, West Lafayette, Indiana.

HAMIELEC, A. E. & RAAL, J. D. 1969 Numerical studies of viscous flow around circular cylinders. *Phys. Fluids* **12**, 11.

INGHAM, D. B. 1968 Note on the numerical solution for unsteady viscous flow past a circular cylinder. *J. Fluid Mech.* **31**, 815.

INGHAM, D. B. 1983 Steady flow past a rotating cylinder. *Comput. Fluids* **11**, 351.

JACKSON, C. P. 1987 A finite element study of the onset of vortex shedding in flow past variously shaped bodies. *J. Fluid Mech.* **182**, 23.

JAIN, P. C. & SANKARA RAO, K. 1969 Numerical solution of unsteady viscous incompressible fluid flow past a circular cylinder. *Phys. Fluids Suppl.* **12**, II 57.

JORDAN, S. K. & FROMM, J. E. 1972 Oscillatory drag, lift and torque on a circular cylinder in a uniform flow. *Phys. Fluids* **15**, 371.

KAWAGUTI, M. 1953 Numerical solution of the Navier–Stokes equations for the flow around a circular cylinder at Reynolds number 40. *J. Phys. Soc. Japan* **8**, 747.

KAWAGUTI, M. & JAIN, P. C. 1966 Numerical study of a viscous fluid past a circular cylinder. *J. Phys. Soc. Japan* **21**, 2055.

KELLER, H. B. & TAKAMI, H. 1966 Numerical studies of viscous flows about cylinders. In *Numerical Solutions of Nonlinear Differential Equations* (ed. D. Greenspan). Wiley.

LIN, C. L., PEPPER, D. W. & LEE, S. C. 1976 Numerical methods for separated flow solutions around a circular cylinder. *AIAA J.* **14**, 900.

NIEUWSTADT, F. & KELLER, H. B. 1973 Viscous flow past circular cylinders. *Comput. Fluids* **1**, 59.

OKAJIMA, A., TAKATA, H. & ASANUMA, T. 1975 Viscous flow around a rotationally oscillating circular cylinder. *Institute of Space and Aeronautical Science, University of Tokyo Rep.* 532.

ORSZAG, S. A. 1971 Numerical simulation of incompressible flows within simple boundaries: accuracy. *J. Fluid Mech.* **49**, 75.

PANIKKER, P. K. G. & LAVAN, Z. 1975 Flow past impulsively started bodies using Green's function. *J. Comput. Phys.* **18**, 46.

PATEL, V. A. 1976 Time-dependent solutions of the viscous incompressible flow past a circular cylinder by the method of the series truncation. *Comput. Fluids* **4**, 13.

PAYNE, R. B. 1958 Calculations of unsteady viscous flow past a circular cylinder. *J. Fluid Mech.* **4**, 81.

PRAVIA, J. R. & GIORGINI, A. 1985 A spectral finite analytic technique for the numerical integration of the Navier–Stokes equations: the impulsively started circular cylinder at $Re = 3000$. *Tech. Rep.* CE-HSE-85-15. School of Civil Engineering, Purdue University, Indiana.

RINALDO, A. & GIORGINI, A. 1984 A mixed algorithm for the calculation of rapidly varying fluid flows: the impulsively started circular cylinder. *Intl J. Numer. Meth. Fluids* **4**, 949.

ROACHE, P. J. 1976 *Computational Fluid Dynamics.* Hermosa.

ROSHKO, A. 1953 On the development of turbulent wake from vortex streets. *NACA Tech. Note* 2913.

ROSHKO, A. 1954 On the drag and shedding frequency of two-dimensional bluff bodies. *NACA Tech. Note* 3169.

SMITH, F. T. 1979 Laminar flow of an incompressible fluid past a bluff body: the separation, reattachment, eddy properties and drag. *J. Fluid Mech.* **92**, 171.

SMITH, F. T. 1981 Comparisons and comments concerning recent calculations for flow past a circular cylinder. *J. Fluid Mech.* **113**, 407.

SON, J. S. & HANRATTY, T. J. 1969 Numerical solution for the flow around a cylinder at Reynolds numbers of 40, 200, and 500. *J. Fluid Mech.* **35**, 369.

TA PHUOC LOC 1980 Numerical analysis of unsteady secondary vortices generated by an impulsively started circular cylinder. *J. Fluid Mech.* **100**, 111.

TA PHUOC LOC & BOUARD, R. 1985 Numerical solution of the early stage of the unsteady viscous flow around a circular cylinder: a comparison with experimental visualizations and measurements. *J. Fluid Mech.* **160**, 93.

TAKAMI, H. & KELLER, H. B. 1969 Steady two-dimensional viscous flow of an incompressible fluid past a circular cylinder. *Phys. Fluids Suppl.* **12**, II 51.

TAMADA, K., MIURA, H. & MIYAGI, T. 1983 Low-Reynolds-number flow past a cylindrical body. *J. Fluid Mech.* **132**, 445.

THOM, A. 1932 Arithmetical solution of problems in steady viscous flow. *Aero. Res. Comm. R. and M.* 1475.

THOM, A. 1933 The flow past circular cylinders at low speeds. *Proc. R. Soc. Lond.* A **141**, 651.

THOMAN, D. C. & SZEWCZYK, A. A. 1969 Time-dependent viscous flow over a circular cylinder. *Phys. Fluids Suppl.* **12**, II 76.

TRAVIS, J. R. & GIORGINI, A. 1971 Numerical simulation of the Navier–Stokes equations in Fourier space. *Tech. Rep.* 30. Water Resources and Hydromechanics Laboratory, School of Civil Engineering, Purdue University, West Lafayette, Indiana.

TRIANTAFYLLOU, G. S., TRIANTAFYLLOU, M. S. & CHRYSSOSTOMIDIS, C. 1986 On the formation of vortex streets behind stationary cylinders. *J. Fluid Mech.* **170**, 461.

TUANN, S. Y. & OLSON, M. D. 1978 Numerical studies of the flow around a circular cylinder by a finite element method. *Comput. Fluids* **6**, 219.

UNDERWOOD, R. L. 1969 Calculation of incompressible flow past a circular cylinder at moderate Reynolds numbers. *J. Fluid Mech.* **37**, 95.

WU, J. C. & THOMPSON, J. F. 1973 Numerical solutions of time-dependent incompressible Navier–Stokes equations using an integro-differential formulation. *Comput. Fluids* **1**, 197.